Concentrators for Water Waves

Chunyang Li,[1,2] Lin Xu,[1,2,4] Lili Zhu,[2] Siyuan Zou,[2] Qing Huo Liu,[3] Zhenyu Wang,[2,*] and Huanyang Chen[1,†]

[1]*Institute of Electromagnetics and Acoustics and Department of Electronic Science, Xiamen University, Xiamen 361005, China*
[2]*College of Civil Engineering and Architecture, Zhejiang University, Hangzhou 310058, China*
[3]*Department of Electrical and Computer Engineering, Duke University, Durham, North Carolina 27708, USA*
[4]*Institute of Physical Science and Information Technology & Key Laboratory of Opto-Electronic Information Acquisition and Manipulation of Ministry of Education, Anhui University, Hefei 230601, China*

By introducing concepts from transformation optics to the manipulation of water waves, we design and experimentally demonstrate two annular devices for concentrating waves, which employ gradient depth profiles based on Fabry-Pérot resonances. Our measurements and numerical simulations confirm the concentrating effect of the annular devices and show that they are effectively invisible to the water waves. We show that transformation optics is thus an effective framework for designing devices to improve the efficiency of wave energy collection, and we expect potential applications in coastline ocean engineering.

Underpinned by the advent of metamaterials [1–3], transformation optics [4–10] has been developed into a powerful tool to design novel wave-manipulation devices that control electromagnetic (EM), acoustic, elastic, and water waves. Notable examples include invisibility cloaks [11–22], field rotators [23–26], field concentrators [27–32], shifters [33–35], and illusion devices [36,37]. Among them, concentrators are devices whose transformation domain is an annulus, within which the incident waves can be collected without any scattering [27–32]. The designed devices with high concentration efficiency usually come from singular mappings [30]. Therefore, the required material parameters of the transformation domain contain singularities (called "optical voids"), that are challenging to implement experimentally. Nonetheless, we found that a phenomenon equivalent to such an optical void can be achieved by exploring Fabry-Pérot (FP) resonances within periodic metallic slit array structures [30]. This concept can be extended to two-dimensional (2D) situations (with the slits along radial directions) and was successfully realized for reduced parameters at a series of FP resonant frequencies.

In ocean engineering, concentration of water waves is crucial to coastal protection and the collection of wave energy. Current utilization of water wave energy is unsatisfactory. One reason is that the waves at sea level are dispersed, which requires many energy conversion devices to be deployed over a large area for energy collection. A concentrator device for water waves might be helpful in this regard, which is simply inherited from the concept of transformation optics. The key properties of such devices are usually inhomogeneous and anisotropic. The notion of using inhomogeneous properties to control water waves goes back to early devices with variable depth profiles, which mimic the refractive index profiles of mirage effects [38,39]. Anisotropic responses to water waves are less easy to achieve. In our earlier work [26], we used alternating strips of step depth profiles such that the waves will experience different propagation velocities for directions parallel and perpendicular to the strips. To obtain such an effective depth "tensor" for anisotropy, the wavelengths usually need to be much larger than the widths of each strip. However, even with such inhomogeneity and anisotropy, concentrators of water waves based on coordinate transformations are nearly impossible to construct, as they require not only a strongly anisotropic water depth distribution but also significantly different gravitational acceleration from the natural environment [22].

In this Letter we introduce gradient depth profiles of extreme anisotropy—namely, waves that propagate only along a specific direction—based on FP resonances to manipulate water waves. We design and fabricate two annular concentrator devices of different sizes. Here waves propagate only along radial directions, which we will show in the following section. The gradient depth profiles help to reduce the scattering at the inner and outer boundaries [38,39]. The FP resonance, well known for optical cavities, can maintain the phase of the waves while keeping perfect transmission. Our experimental measurements and simulation results confirm the concentrating and invisibility effect of these two devices.

Construction of concentrators for water waves.—Given the similarity of the field equation of water waves with that of 2D EM waves, we apply a concentrator design with extreme anisotropy based on FP resonances [30] to water waves. A schematic plot of the concentrator is shown in Fig. 1(a) (top view and cross-section view). The region outside the radius r_o is the environment with a depth of
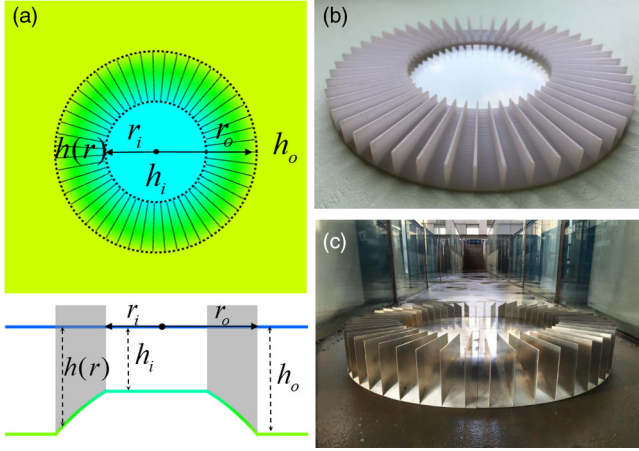
FIG. 1. The schematic diagram and the two devices. (a) The top view and cross section of the schematic diagram of concentrator with a gradient depth profile. The small and large concentrators are shown in (b) and (c), respectively.

water h_o, while the region inside the radius r_i has a water depth h_i. The region between r_o and r_i is of extreme anisotropy based on FP resonances, which consists of gradient depth $h(r)$ of water separated by a series of radial slits. The slits are higher than the wave surface, so the waves can only propagate along radial directions: this is what we mean by extreme anisotropy. The main property of such a configuration is that the depth is chosen to be continuous at each point, namely,

$$h(r_o) = h_0 \quad \text{and} \quad h(r_i) = h_i.$$

It is thereby much easier to implement a continuous depth profile for water waves than a refractive index profile for EM waves [30].

Prior to modeling the real device, we take a shallow water approximation [20,40–42] so that the linear dispersion relation can be written as

$$\omega = \sqrt{ghk}, \tag{1}$$

where ω, g, h, and k represent the angular frequency, the gravitational acceleration, water depth, and the wave number of the water waves, respectively. Suppose the wave number of water waves in the region outside the radius r_0 is k_0, and the effective refractive index of the region inside radius r_i should be

$$n_i = k/k_0. \tag{2}$$

According to Eqs. (1) and (2), we obtain

$$n_i = \sqrt{h_o/h_i}, \tag{3}$$

where we assume that the refractive index of the region outside the radius r_o is 1, namely, $n_o = 1$. The refractive index of the region inside the radius r_i is thereby $n_i = r_o/r_i$

based on the design of concentrators [30]. The choice of the refractive index in the region between r_i and r_o can be quite flexible. Here, we select a relation for experimental fabrication, namely,

$$n(r) = \frac{r_o - r}{r_i} + 1. \tag{4}$$

According to Eqs. (3) and (4), we can obtain the distribution of water depths,

$$\begin{aligned} h_i &= h_0(r_i/r_o)^2, & r < r_i, \\ h(r) &= \frac{h_0 r_i^2}{(r_o - r + r_i)^2}, & r_i < r < r_o. \end{aligned} \tag{5}$$

The invisibility effect of the concentrator occurs at FP resonance conditions, where the wavelength of water waves λ should satisfy [30]

$$\int_{r_i}^{r_o} n(r)dr = m\frac{\lambda}{2}, \qquad m = 1, 2, 3, \ldots \tag{6}$$

that is, the "optical path" is an integer multiple of half a wavelength. Hence, waves can be perfectly transmitted through each small channel with no phase delay.

With these parameters, we construct two annular concentrator devices of different sizes to demonstrate the concentrating and invisibility effect of water waves, as shown in Figs. 1(b) and 1(c), respectively.

The smaller annular concentrator is fabricated by a 3D printer with outer radius $r_o = 70$ mm, inner radius $r_i = 35$ mm and environmental water depth $h_0 = 8$ mm. In the region between radius r_o and r_i, the gradient refractive index varies from 1 to 2. Meanwhile, we evenly arrange fifty thin baffles of thickness 1.1 mm on the annulus to form a slit array. The slit width near the radius r_o is 7.7 mm, while close to the radius r_i it is 3.3 mm. We put a piece of plastic of thickness 6 mm into the region inside the radius r_i such that the depth becomes $h_i = 2$ mm, which can achieve an effective refractive index of 2 according to Eq. (3).

The configuration of the bigger annular concentrator in a deeper water tank is shown in Fig. 1(c). Its parameters are outer radius $r_o = 42.888$ cm, inner radius $r_i = 24.761$ cm, environmental water depth $h_0 = 10$ cm. Similarly, we evenly arrange fifty thin baffles of thickness 0.5 mm on the annulus to form the slit array. The slit width near the radius r_o is 5.34 cm, while close to the radius r_i it is 3.06 cm. A cylinder of thickness 6.667 cm is located in the region inside the radius r_i, which can achieve an effective refractive index of 1.732.

Invisibility and concentrating effect of concentrators.— The above devices are designed using the shallow water approximation such that the field equation will be identical to Maxwell's equations in two dimensions. However, the

wavelength should be more than 20 times the water depth for this approximation. For both cases, we remodel the devices during the simulation using the transcendental dispersion relationship

$$\omega^2 = gk \tanh(kh), \qquad (7)$$

to obtain effective water depths or effective refractive index profiles [26].

For the small annular concentrator, we mainly focus on demonstrating the invisibility effect. We make measurements of this device based on the experimental setup described previously [22,26,35,40–46]. For a frequency of 4.95 Hz, which is appropriate to the FP resonance for $m = 2$, the amplitude profile is shown in Fig. 2(a) with a background wavelength of 50 mm. It is evident that the water waves are plane waves both inside and outside the concentrator, which demonstrates the invisibility effect: there is essentially no scattering. The waves were attenuated after passing through the concentrator because of the fluid-solid interaction. We also perform simulations of wave amplitudes using commercial software (COMSOL Multiphysics) with the linear dispersion relationship Eq. (1) and the transcendental dispersion relationship Eq. (7). Figure 2(b) shows results for the linear dispersion relationships, illustrating the perfect invisibility effect (the background wavelength is 52.5 mm). Figure 2(c) is for the transcendental dispersion relationship; in this case the invisibility effect is compromised (the background
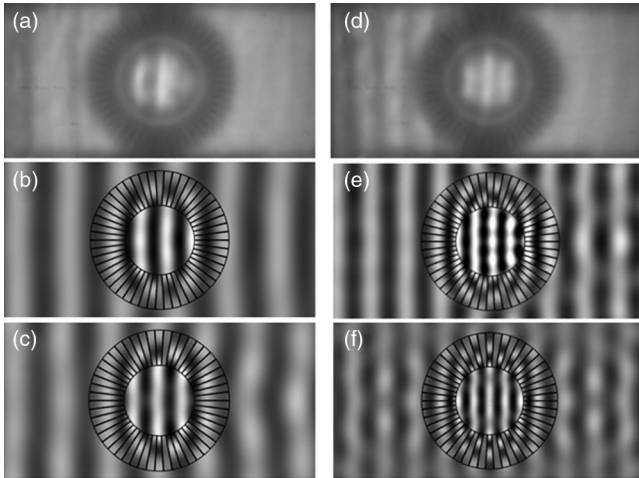

FIG. 2. The wave amplitudes of experimental measurements and simulation results for the small concentrator. For $m = 2$, (a) is the experimental measurement with a background wavelength of 50 mm, (b) is the simulation result with the linear dispersion and a background wavelength of 52.5 mm, (c) is the simulation result with the transcendental dispersion and a background wavelength of 48.5 mm. For $m = 3$, (d) is the experimental measurement with a background wavelength of 31 mm, (e) is the simulation result with the linear dispersion and a background wavelength of 35 mm, (f) is the simulation result with the transcendental dispersion and a background wavelength of 29.7 mm.

wavelength is 48.5 mm). The effective refractive index of the region inside radius r_i for the transcendental dispersion has changed from 2 to about 1.8. According to the corresponding principle in transformation optics, the device is "seen" by the waves as an object with an effective refractive index of about 0.9—hence the slight scattering. Under the working frequency of 7.05 Hz, corresponding to the FP resonance for $m = 3$, the measured amplitude profile is shown in Fig. 2(d) for a background wavelength of 31 mm. Figures 2(f) and 2(f) are for the linear dispersion relationship and the transcendental dispersion relationship, respectively. Their background wavelengths are shifted to 35 and 29.7 mm, respectively. As the effective refractive index tensor (or depth "tensor") in the region between r_i and r_o is more accurate when the wavelength is much larger than the width of slits [26], the invisibility effect is less than perfect for Fig. 2(e), while for Fig. 2(f) the scattering gets even stronger. That is because the effective refractive index of the region inside radius r_i for the transcendental dispersion has changed to about 1.6, corresponding to an illusion with an effective refractive index of about 0.8. Hence, the device at larger wavelengths seems to have better invisibility according to the simulation results, as the effective refractive index of the illusion is closer to that of the background and the theory of effective refractive index tensor is more accurate. To obtain the amplitude magnification factor of the inner part of the concentrator, we perform a pixel analysis for the experimental photographs (similar to that in Ref. [42]). The amplitude magnification factors inside radius r_i for $m = 2$ and 3 are 2.21 and 1.94, respectively, consistent with the simulation results (we normalize them to the amplitude of incident waves). In addition, the background wavelength from the measurement ranges between those from the linear and transcendental dispersions, which is due to the effect of considering the dispersion of $\omega^2 = gk \tanh(kh)(1 + k^2 d_c^2)$ (where d_c is capillary length, and $d_c = 2.7$mm for water).

For the big concentrator, a large water tank 60 m long, 1.2 m wide, and 2 m deep was used for experimental testing. A push-type wave maker is arranged at one end of the tank and a wave dissipating device at the other end. To demonstrate the concentrating effect of the big concentrator, we measure the amplitude around the concentrator by using wave gauges rather than taking photos. First, for the concentrator with and without baffles we plot the amplitude magnification factors for a single point inside the radius r_i from 1.1 to 1.75 Hz when the incident amplitude is 1.2 mm, as shown in Fig. 3(a). For the corresponding simulations we plot the amplitude magnification factors for a single point and the average area inside radius r_i from 1.1 to 1.75 Hz, as shown in Figs. 3(b) and 3(c), respectively. We find that the big concentrator has maximal values of amplitude inside radius r_i at frequency 1.5 Hz, which demonstrates the concentrating effect of the above design at one of the FP resonances. Amplitude
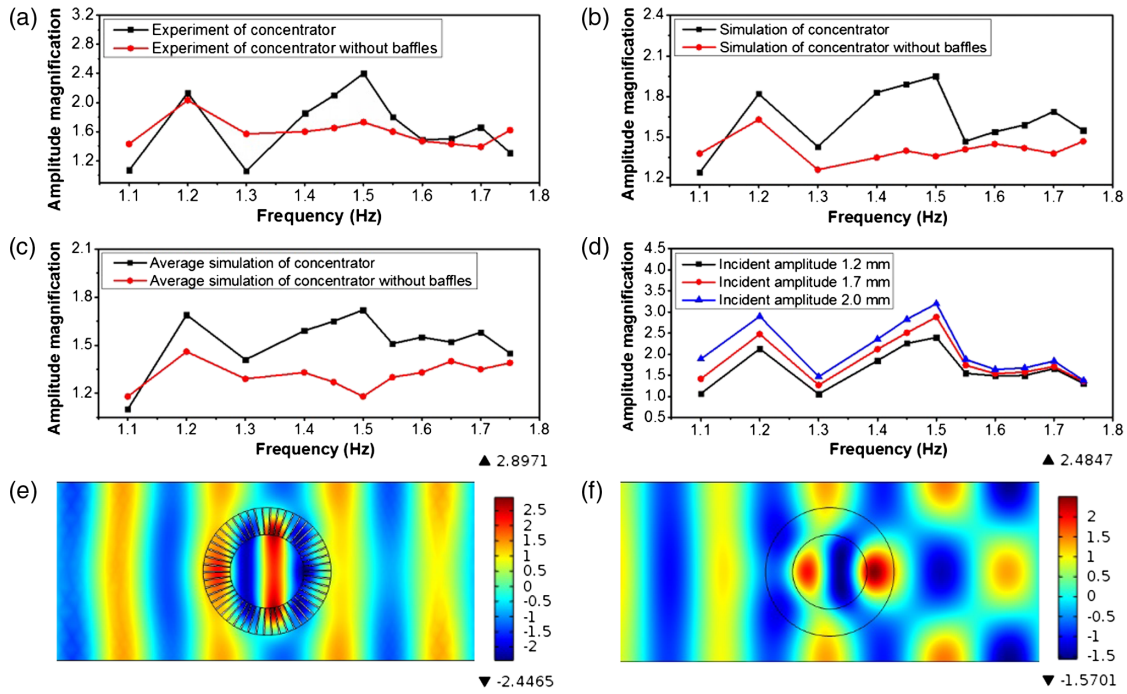
FIG. 3. (a) The experimental amplitude magnification factors of the concentrator with and without baffles from 1.1 to 1.75 Hz for incident amplitude of 1.2 mm. (b) The simulated amplitude magnification factors of a single point. (c) The simulated averaged amplitude magnification factors for the inner part. (d) The amplitude magnification factors of the inner part from 1.1 to 1.75 Hz for incident amplitude of 1.2 (black), 1.7 (red), and 2 mm (blue) for the big-size concentrator, respectively. (e) The simulated amplitude profiles of concentrator with baffles at the frequency of 1.5 Hz. (f) The simulated amplitude profiles of concentrator without baffles at the frequency of 1.5 Hz.

magnification factors at various frequencies from experiments are basically consistent with those from the simulations. This is because the incident amplitude of water wave is 1.2 mm, which approximately satisfies the condition of linear amplitude waves: nonlinearities are negligible. The amplitude magnification factor inside radius r_i is about 2, which is close to the theoretical value. However, when the incident amplitudes increase to 1.7 and 2 mm, the nonlinear effect grows stronger and the amplitude magnification factors inside radius r_i are larger, which deviates from the theoretical value. We plot the amplitude magnification factors inside radius r_i of the concentrator from 1.1 to 1.75 Hz when the incident amplitudes of water waves are 1.2, 1.7, and 2 mm, respectively, as shown in Fig. 3(d). The nonlinear effect here is helpful as it makes magnification factors larger for the whole frequency range. In addition, we plot the corresponding simulation patterns of the concentrator with and without baffles, as shown in Figs. 3(e) and 3(f) for incident amplitude of 1.2 mm and at the frequency of 1.5 Hz. The invisibility and concentrating effect is again well demonstrated.

In order to visualize the concentrating effect of the big concentrator, we put a small boat onto the water surface in the environment and the inner part of the concentrator, respectively. The amplitude of water waves can be represented by the vertical movement of the boat, while its horizontal movement is confined by ropes fixed to the bottom as shown in Fig. 4(a). We put a sensor at the

position of the boat to obtain its amplitude of vertical movement. The amplitude of water wave in the environment is 2 mm in Fig. 4(a), which is marked with a black arrow. The amplitudes in the inner part of the concentrator with incident wave of frequencies from 1.1 to 1.7 Hz are shown in Figs. 4(b)–4(g), which correspond to the blue curve of Fig. 3(d). We also present the related videos of the movement of the boat inside the big concentrator, from 1.1 to 1.7 Hz with the incident wave amplitude of 2 mm, in the Supplemental Material [47].
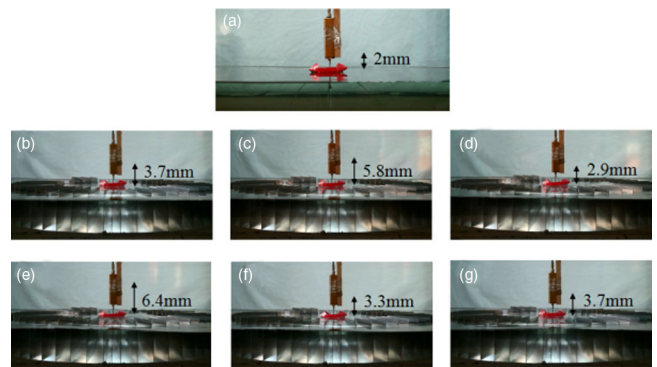

FIG. 4. Screenshots from experimental videos. (a) The boat with the incident wave amplitude of 2 mm. The boat in the inner part of the concentrator at the frequency of (b) 1.1, (c) 1.2, (d) 1.3, (e) 1.5, (f) 1.6, and (g) 1.7 Hz.

In conclusion, we have successfully designed and fabricated two annular concentrator devices for water waves by using gradient depth profiles based on Fabry-Pérot resonances. Our experimental measurements and simulated results demonstrate the concentrating and invisibility effect of these concentrators. Our findings indicate that the slit array structure under Fabry-Pérot resonances can be used to manipulate water waves. Nonlinearities can help this design. Our approach could have significant value for harvesting water wave energy and for deepening our understanding of the propagation mechanisms of water waves.

---

[*]wzyu@zju.edu.cn
[†]kenyon@xmu.edu.cn

[1] D. R. Smith, W. J. Padilla, D. C. Vier, S. C. Nemat-Nasser, and S. Schultz, Phys. Rev. Lett. **84,** 4184 (2000).

[2] R. A. Shelby, D. R. Smith, and S. Schultz, Science **292,** 77 (2001).

[3] R. A. Shelby, D. R. Smith, S. C. Nemat-Nasser, and S. Schultz, Appl. Phys. Lett. **78,** 489 (2001).

[4] U. Leonhardt, Optical conformal mapping, Science **312,** 1777 (2006).

[5] J. B. Pendry, D. Schurig, and D. R. Smith, Science **312,** 1780 (2006).

[6] Z. Y. Wang, Y. Luo, W. Z. Cui, W. Ma, L. Peng, J. T. Huangfu, H. S. Chen, and L. X. Ran, Appl. Phys. Lett. **94,** 234101 (2009).

[7] N. I. Landy, N. Kundtz, and D. R. Smith, Phys. Rev. Lett. **105,** 193902 (2010).

[8] H. Y. Chen, C. T. Chan, and P. Sheng, Nat. Mater. **9,** 387 (2010).

[9] B.-I. Popa and S. A. Cummer, Phys. Rev. A **84,** 063837 (2011).

[10] L. Xu and H. Y. Chen, Nat. Photonics **9,** 15 (2015).

[11] D. Schurig, J. J. Mock, S. A. Cummer, J. B. Pendry, A. F. Starr, and D. R. Smith, Science **314,** 977 (2006).

[12] J. Li and J. B. Pendry, Phys. Rev. Lett. **101,** 203901 (2008).

[13] T. Ergin, N. Stenger, P. Brenner, J. B. Pendry, and M. Wegener, Science **328,** 337 (2010).

[14] D. Shin, Y. Urzhumov, Y. Jung, G. Kang, S. Baek, M. Choi, H. Park, K. Kim, and D. R. Smith, Nat. Commun. **3,** 1213 (2012).

[15] S. Zhang, C. G. Xia, and N. Fang, Phys. Rev. Lett. **106,** 024301 (2011).

[16] G. Dupont, M. Farhat, A. Diatta, S. Guenneau, and S. Enoch, Wave Motion **48,** 483 (2011).

[17] M. Farhat, S. Guenneau, and S. Enoch, Phys. Rev. Lett. **103,** 024301 (2009).

[18] N. Stenger, M. Wilhelm, and M. Wegener, Phys. Rev. Lett. **108,** 014301 (2012).

[19] T. M. Chang, G. Dupont, S. Enoch and S. Guenneau, New J. Phys. **14,** 035011 (2012).

[20] G. Dupont, O. Kimmoun, B. Molin, S. Guenneau, and S. Enoch, Phys. Rev. E **91,** 023010 (2015).

[21] M.-R. Alam, Phys. Rev. Lett. **108,** 084502 (2012).

[22] A. Zareei and M.-R. Alam, J. Fluid Mech. **778,** 273 (2015).

[23] H. Y. Chen and C. T. Chan, Appl. Phys. Lett. **90,** 241105 (2007).

[24] Y. Luo, J. J. Zhang, B.-I. Wu, and H. S. Chen, Phys. Rev. B **78,** 125108 (2008).

[25] H. Y. Chen, B. Hou, S. Y. Chen, X. Y. Ao, W. J. Wen, and C. T. Chan, Phys. Rev. Lett. **102,** 183903 (2009).

[26] H. Y. Chen, J. Yang, J. Zi, and C. T. Chan, Europhys. Lett. **85,** 24004 (2009).

[27] M. Rahm, D. Schurig, D. A. Roberts, S. A. Cummer, D. R. Smith, and J. B. Pendry, Photonics Nanostruct. Fundam. Appl. **6,** 87 (2008).

[28] C. Navau, J. Prat-Camps, and A. Sanchez, Phys. Rev. Lett. **109,** 263903 (2012).

[29] M. M. Sadeghi, H. Nadgaran, and H. Y. Chen, Front. Phys. **9,** 90 (2014).

[30] M. M. Sadeghi, S. Li, L. Xu, B. Hou, and H. Y. Chen, Sci. Rep. **5,** 8680 (2015).

[31] M. M. Sadeghi, X. Lin, H. Nadgaran, and H. Y. Chen, Sci. Rep. **5,** 11015 (2015).

[32] J. J. Yang, M. Huang, C. F. Yang, and G. H. Cai, J. Vib. Acoust. **133,** 061016 (2011).

[33] W. X. Jiang, T. J. Cui, X. Y. Zhou, X. M. Yang, and Q. Cheng, Phys. Rev. E **78,** 066607 (2008).

[34] C. P. Berraquero, A. Maurel, P. Petitjeans, and V. Pagneux, Phys. Rev. E **88,** 051002 (2013).

[35] Z. Y. Wang, P. Zhang, X. F. Nie, and Y. Q. Zhang, Sci. Rep. **5,** 16846 (2015).

[36] Y. Lai, J. Ng, H. Y. Chen, D. Z. Han, J. J. Xiao, Z. Q. Zhang, and C. T. Chan, Phys. Rev. Lett. **102,** 253902 (2009).

[37] Z. Xiong, L. Xu, Y. D. Xu, and H. Y. Chen, Front. Phys. **12,** 124202 (2017).

[38] F. Bampi and A. Morro, Il Nuovo Cimento 1C **1,** 377 (1978).

[39] F. Bampi and A. Morro, Il Nuovo Cimento 2C **2,** 352 (1979).

[40] X. H. Hu and C. T. Chan, Phys. Rev. Lett. **95,** 154501 (2005).

[41] X. Hu, C. T. Chan, K.-M. Ho, and J. Zi, Phys. Rev. Lett. **106,** 174501 (2011).

[42] Z. Wang, C. Li, R. Zatianina, P. Zhang, and Y. Zhang, Phys. Rev. E **96,** 053107 (2017).

[43] X. H. Hu, Y. F. Shen, X. H. Liu, R. T. Fu, and J. Zi, Phys. Rev. E **69,** 030201(R) (2004).

[44] C. Zhang, C. T. Chan, and X. H. Hu, Sci. Rep. **4**, 6979 (2014).

[45] Z. Y. Wang, P. Zhang, Y. Q. Zhang, and X. F. Nie, Physica (Amsterdam) **431B**, 75 (2013).

[46] Z. Y. Wang, X. F. Nie, and P. Zhang, Phys. Scr. **89**, 095201 (2014).

[47] See Supplemental Material at http://link.aps.org/supplemental/10.1103/PhysRevLett.121.104501 for the experimental videos at the corresponding frequencies from 1.1 Hz to 1.7 Hz when the incident wave amplitude is 2 mm.